Int. J. Electrochem. Sci., 8 **(2013)** 10601 - 10620

International Journal of ELECTROCHEMICAL SCIENCE
www.electrochemsci.org

The Role of a Layer-by-Layer Film Containing Pt Nanoparticle on the Performance of a Glucose Enzymatic Biosensor

Vagner dos Santos, Monalisa dos Santos, Cliciane Guadalupe de Jesus, Sérgio Toshio Fujiwara, Jarem Raul Garcia, Christiana Andrade Pessôa, Karen Wohnrath[*]

Departamento de Química, Universidade Estadual de Ponta Grossa, 84030-900, Ponta Grossa - PR, Brazil
[*]E-mail: karen.woh@gmail.com

Received: 19 May 2013 / *Accepted:* 2 July 2013 / *Published:* 1 August 2013

A novel glucose biosensor based on immobilization of glucose oxidase in LbL films containing platinum nanoparticles (PtNPs) nanohybrid incorporated in 3-*n*-propylpyridinium silsesquioxane chloride ($SiPy^+Cl^-$) was developed. These films were assembled with the poly(2,5-methoxypropyloxy sulphonatephenylenevinylene) (PPV-SO_3) as polyanion alternated with the (Pt-$SiPy^+Cl^-$) nanohybrid polycation to obtain the (PPV/Pt-$SiPy^+Cl^-$)$_n$ and (Pt-$SiPy^+Cl^-$/PPV)$_n$ LbL films. The formation of these LbL films was monitored by linear increase observed in the absorbance in the UV-Vis spectra and the number of Pt-$SiPy^+Cl^-$/PPV (R =0.994) or PPV/Pt-$SiPy^+Cl^-$ (R = 0.997) bilayers. FTIR and Raman spectra confirmed the presence of the polyelectrolytes in the LbL films. The films were electrochemically studied using phosphate buffer saline (PBS) solution 0.1 mol L^{-1} (pH 7.0), and it was observed that the (PPV/Pt-$SiPy^+Cl^-$)$_6$ LbL films containing 6 bilayers showed better performance in H_2O_2 detection with Ipa = 6.16 μA and Epa = 1.06 V. Thus, glucose oxidase (GOx) was immobilized onto (PPV/Pt-$SiPy^+Cl^-$)$_6$ LbL film surface to obtain the (PPV/Pt-$SiPy^+Cl^-$)$_6$GOx biosensor. The properties of the resulting glucose biosensor were studied by amperometric measurements. The biosensor displayed good repeatability and reproducibility with a sensitivity of 1.17 μA/mmol L^{-1} cm^{-2}, a detection limit (DL) of 27.4 μmol L^{-1} and a quantification limit (QL) of 91.4 μmol L^{-1}. In addition, the resulting glucose biosensor exhibited a constant electrochemical answer to glucose for a period of approximately 30 days, thus indicating a stable adsorption of GOx. The apparent Michaelis-Menten constant (k_m^{app}) obtained was of 2.64 mmol L^{-1}, this is an excellent value compared to those obtained with hybrid materials due to PtNPs available in the structure of the $SiPy^+Cl^-$ which increase the surface area.

Keywords: silsesquioxane, platinum nanoparticles, LbL films, glucose oxidase, and hydrogen peroxide.

1. INTRODUCTION

Materials based on silsesquioxane structures have been successfully utilized in the development of electrochemical sensors [1,2,3]. The silsesquioxanes are nanostructured molecules that can be formed as random, ladder, cage, or partial cage structures [4]. These compounds containing the empirical formula $(RSiO_{1.5})n$, where R is a hydrogen atom or organic functional group such as an hydroxyl, alkyl, acrylate, hydroxyl, alkylene, acrylate, hydroxyl, or epoxide unit [4]. The *n* is an integer number that can vary with values equal or greater than 4, however it is more used 6, 8 or 10 [1,5]. These organic substituents have an important role in the structure because several properties are attributed to reactions of these groups [1].

Among the various classes of silsesquioxane, the 3-n-propylpyridinium silsesquioxane chloride ($SiPy^+Cl^-$), exhibits excellent properties for the formation of films [6], strong anionic exchange capacity [7], high solubility in water [8,9] and excellent ability to act as a nanoreactor for the synthesis of metallic nanoparticles (NPs) [6,10].

Recently some works with metallic NPs incorporated into silsesquioxane are reported as the performed by Menezes et al [11] that prepared gold nanoparticles (AuNPs) lower than 10 nm using two charged silsesquioxanes, the $SiPy^+Cl^-$ and the propyl-1-azonia-4-azabicyclo[2.2.2]octane chloride ($SiDb^+Cl^-$), as stabilizer agents. The AuNPs/silsesquioxane systems were immobilized in a silica matrix coated with aluminum oxide used to prepare carbon paste electrodes (CPEs) for the electrooxidation of nitrite. The electrode Au-$SiPy^+Cl^-$ showed the higher oxidation current to nitrite and this behaviour was attributed to AuNPs that helped in a fast electron transfer compared with the other electrodes without AuNPs. The Au-$SiDb^+Cl^-$ electrode exhibited lower oxidation currents when compared to the Au-$SiPy^+Cl^-$, which was attributed to the difference in the structure of silsesquioxane because while the $SiDb^+Cl^-$ is aliphatic , the $SiPy^+Cl^-$ presents aromatic π electrons that may contribute to the conductivity.

In the another work realized by Santos et al [6], the $SiPy^+Cl^-$ was used as a nanoreactor of platinum NPs (PtNPs) for the preparation of modified electrode by Layer-by-Layer (LbL) technique. These electrodes were applied as electrochemical sensor to dopamine (DA) in the presence of the ascorbic acid (AA) interferent. The PtNPs were crucial in oxidation process of DA because with the electrode $(PVS/Pt\text{-}SiPy^+Cl^-)_3$ containing 3 bilayers where the PVS is poly(vinyl sulfonic acid), it was observed an increase of the oxidation current to DA and a higher difference in the oxidation potential of the DA and the AA (ΔE = 550 mV). This difference is higher than the observed in the work of Jesus et al [3], that observed a difference in the oxidation potential of the DA and the AA about to 500 mV obtained with an electrode formed by 5 bilayers of copper (II) tetrasulfophthalocyanine (CuTsPc) and $SiPy^+Cl^-$ $(SiPy^+Cl^-/CuTsPc)_5$ without NPs.

In a recent study, the detection of encapsulated DA into liposomes was also investigated by Santos et al [10]. The authors observed a decrease in the difference of oxidation potential of the DA and the AA and uric acid (UA) interferents of 630 to 320 mV obtained with o $(PPV/Pt\text{-}SiPy^+Cl^-)_3$ containing 3 bilayers where the PPV is sulphonate *p*-phenylenevinylene. This behavior was explained by the approximation of the liposomes to electrode surface which can influences in the interaction between the PtNPs into $SiPy^+Cl^-$ and the AA and AU interferences generating a competitive process.

In addition of the use of NPs in electrochemical sensors, their application in the constitution of biosensors has increased considerably showing large signal enhancements and lower detection limits [12,13]. Due to their simplicity and speed, several amperometric glucose biosensors have been used for glucose detection. These biosensors are based on the immobilization of glucose oxidase (GOx) and determining enzymatically liberated hydrogen peroxide (H_2O_2) by electrochemical methods [14]. However, there are some problems, such as low sensitivity and stability, and narrow linear range, which cannot produce the desired detection [15]. Thus, in order to solve these problems and improve the performance of these biosensors, significant research has been devoted to this field by addition of redox mediators such as ferrocene [16,17], Prussian Blue [18], carbon nanotubes [19,20,21], conducting polymers [22,23], and nanoparticles [14,24,25]**Error! Bookmark not defined.**.

It is generally accepted that biosensor containing platinum nanoparticles (PtNPs) are biocompatible and have excellent catalytic capabilities towards the oxidation and reduction of H_2O_2 due to their large active surface area and lattice planes compare to bulk [25]. Furthermore, the fact that the reaction of PtNPs facilitates electron transfer from H_2O_2, is very attractive for the construction of oxidase-based enzymatic biosensors using PtNPs, as seen in other studies [14,15,25]. Aiming to avoid agglomerations and retain activity, PtNPs are generally dispersed on a conducting support [26]. Thus, an advantageous technique for this purpose has been the immobilization of NPs by the LbL technique. This technique provides the possibility of minimizing protein denaturing because the adsorption process is carried out in aqueous solutions, under mild conditions [27]. In addition, the LbL technique represents a promising and environmentally friendly preparation method because no complicated instruments or chemical reactions are involved [14]. The incorporation of nanomaterial into a sensing device has been used extensively to improve the conductivity of composition films [28] and greatly increases the biosensor sensitivity and response speeds due to its high chemical stability, high surface area, and unique electronic properties [19].

The high sensitivity, potential selectivity, low cost and possibility of miniaturization/automation of the enzymatic biosensors are the factors responsible for the application of these analytical devices in chemistry and biology [27]. Wu et al [29] describe a new strategy for fabricating glucose biosensor by LbL technique containing chitosan (CS), AuNPs, poly(allylamine) and GOx on Pt electrode. The biosensor containing 6 bilayers showed higher amperometric response with a wide linear range of 0.5 - 16 mM and a detection limit (DL) of 7.0 μM. These results proved that AuNPs could firmly immobilize more GOx in multilayer films due to their large specific surface areas, and provide conduction pathway to accelerate electron transfer due to their excellent conductivity.

Several studies show that the immobilization of metallic nanoparticles (NPs) in LbL films has been crucial for the electrochemical detection of glucose [14,25,30]. Tsai, M. C. and Tsai, Y. C. [30] noted that the performance exhibited by the GOx-Pt-MWCNT-ACS biosensor, where MWCNT is multiwalled carbon nanotubes and ACS is alumina-coated silica, including a wide linear range of up to 10.5 mmol L^{-1} and a high sensitivity level of 113.13 mA/mmol L^{-1} cm^{-2}, could be attributed to the presence of PtNPs combined with MWCNTs that increase the surface area in the electrode. Jiang, X. et al [14] immobilized GOx on mesoporous carbon (OMC) supporting PtNPs by entrapment in electropolymerized pyrrole film. The PtNPs were crucial in the performance of the biosensor in

relation to OMC because it improved the analytical performance in terms of low detection limit (0.05 mmol L^{-1}), high sensitivity (0.38 μA/mmol L^{-1}), and wide linear range (0.05 - 3.70 mmol L^{-1}).

Platinum (PtNPs) and palladium (PdNPs) nanoparticles were used by Lu et al [31] in the fabrication of graphite nanoplatelets, in order to increase the electroactive area of the electrode and decreased the overpotential in the detection of H_2O_2, obtaining a very fast biosensor (2 s in response), with low production costs. In addition, high selectivity was demonstrated for the nanoparticles-based biosensor, in comparison with the biosensor without nanoparticles. Indeed, addition of AA or UA to glucose solution resulted in a 56% and 125% increase in the biosensor output, respectively, for the biosensor without nanoparticles. On the other hand, an increase of 8% to 18% was provided for the nanoparticles-based biosensor, indicating an increased selectivity.

The influence of metallic NPs into $SiPy^+Cl^-$ was not investigated in enzymatic biosensor containing GOx. For this reason, this paper reports the building of a glucose biosensor based on the adsorption of glucose oxidase (GOx) onto the surface containing PtNPs incorporated into $SiPy^+Cl^-$. The nanohybrid formed was alternated with poly(2,5-methoxypropyloxy sulphonatephenylenevinylene) PPV-SO_3 in the process of preparation of LbL films. These polyelectrolytes were selected as the building blocks to assemble $(PPV/Pt\text{-}SiPy^+Cl^-)_n$ and $(Pt\text{-}SiPy^+Cl^-/PPV)_n$ LbL films on the surface of a glass substrate coated with fluorine-doped tin oxide (FTO) for electrochemical characterization of these films. These studies were performed in order to improve the electrocatalytic behaviour for hydrogen peroxide, which is released by the action of GOx upon glucose. The performance of the prepared glucose biosensor with respect to sensitivity, linear range, response time and detection limit is presented and discussed.

2. EXPERIMENTAL

2.1 Synthesis of the Pt-$SiPy^+Cl^-$ nanohybrid

The synthesis of the Pt-$SiPy^+Cl^-$ nanohybrid was realized according to a procedure similar to that described in the literature [6,10]. In order to incorporate the PtNPs into $SiPy^+Cl^-$ (BR9803053-A), 10 mL of 2 mmol L^{-1} H_2PtCl_6 (Aldrich Co) was mixed with 10 mL of 2 g L^{-1} aqueous solution of $SiPy^+Cl^-$ and 10 mL of 0.5 mol L^{-1} formic acid (Mallinckrodt), which was used as the reducing agent. The solution was mixed for 12 hours at room temperature under magnetic stirring until the Pt-$SiPy^+Cl^-$ nanohybrid was obtained.

Measurements of dynamic light scattering (DLS) and Zeta potential were performed with the Pt-$SiPy^+Cl^-$ solution to verify the distribution, size and stability of the PtNPs in the $SiPy^+Cl^-$. These DLS measurements were performed using Microtac Zetatrac equipment.

2.2 Film Assembly

The fabrication of LbL films was based on electrostatic attraction between the PPV-SO_3 and Pt-$SiPy^+Cl^-$ used as polyanion and polycation, respectively. The multilayer deposition was performed

manually by immersing the substrate alternately into the Pt- $SiPy^+Cl^-$ and 2.5 g L^{-1} PPV-SO_3 solutions (with pH values of 2.9 and 5.5, respectively) for 4 min. After deposition of each layer, the substrate was rinsed with water for 10 s to remove excess non-adsorbed molecules and then dried in air. This procedure was repeated until the desired number of bilayers was formed. The pH of the washing solutions were adjusted to the pH values of the polyelectrolyte solutions. Films were produced in two different deposition sequences, $(Pt\text{-}SiPy^+Cl^-/PPV)_n$ and $(PPV/Pt\text{-}SiPy^+Cl^-)_n$, with the bilayer number equal to *n*. The films were deposited onto FTO-coated glass substrates (Flexitec, R_s=10–20 Ωm), quartz, Si and silver (colloidal dispersion on the glass).

The immobilization of GOx (extracted from *Aspergillusniger*, 155000 U/g solid, Sigma Aldrich) was performed by immersion of a $(PPV/Pt\text{-}SiPy^+Cl^-)_6$ LbL film, containing 6 bilayers, into a GOx solution 2 mg mL^{-1} at pH 7 in phosphate buffer saline (PBS) for 5 and 30 min, where the negatively charged GOx (pI = 4.6) was adsorbed onto the positively charged Pt-$SiPy^+Cl^-$ surface through electrostatic interactions. The loosely attached GOx molecules were removed from the surface by immersion of $(PPV/Pt\text{-}SiPy^+Cl^-)_6$GOx into PBS buffer, pH 7. The films were prepared and kept at 4 °C.

2.3 Characterization of the Layer-by-layer Films

The growth of the multilayers was monitored via UV-Vis spectroscopy (Cary 50 BIO) using $(PPV/Pt\text{-}SiPy^+Cl^-)_n$ and $(Pt\text{-}SiPy^+Cl^-/PPV)_n$ films containing 3, 6, 9, 12, 15, 18, 21, 24, 27 and 30 bilayers deposited onto quartz substrates. Further measurements of UV-Vis spectroscopy were performed in order to evaluate the kinetic study of the deposition of the polyelectrolytes and monitor the formation of PtNPs.

Fourier transform infrared spectroscopy (FTIR) measurements were carried out on the $(PPV/Pt\text{-}SiPy^+Cl^-)_{30}$ LbL films, and the PPV-SO_3, $SiPy^+Cl^-$ and Pt-$SiPy^+Cl^-$ drop-coated films deposited onto Si substrates using a Shimadzu model 8400 FTIR in transmission mode. Spectra were collected in the range of 400 to 4000 cm^{-1}at 4cm^{-1} resolution, with 64-time scans. Raman scattering measurements (Stray Raman Bruker/Senterra) were carried out on the films deposited onto the silver substrate. Spectra were collected in the range of 45 to 3700 cm^{-1} at 2 mW of power, with a green laser of wavelength 532 nm, and with 3-time scans.

Film morphology analyses were carried out with an atomic force microscope (AFM) (Shimadzu SPM 9500-J3), in non-contact mode with a Silicon SPM-Sensor (Al-coating) (Nano Word) with a thickness of 4 μm, length 125 μm, width 30 μm, resonance frequency of about 320 kHz, and force constant 42 N/m. The software used was SPM manager version 3.03.

Circular dichroism (CD) spectra measurements were performed with GOx 2 mg mL^{-1} pH 7 and with the $(PPV/Pt\text{-}SiPy^+Cl^-)_6$GOx LbL films obtained at different times: 5 and 30 minutes. The aim was to verify the conformational structure of GOx in solution and immobilized on quartz substrate. These measurements were performed in a JascoJ-815 spectrometer with 8 scans per measurement.

For electrochemical characterization, a 30 mL three-electrode electrochemical cell containing a hydrogen electrode as the reference electrode, a Pt plate (1.2 cm^2) as the counter electrode and the LbL

films deposited onto the FTO substrate (fixed area at 0.6 cm^2) as the working electrode were used. Cyclic voltammograms (CVs) were recorded in the potential range of 0.3 to 1.3 V using a 0.1 mol L^{-1} PBS buffer solution (pH 7.0) as the supporting electrolyte with a scan rate of 30 mV s^{-1}. Determination of hydrogen peroxide (H_2O_2) was evaluated by differential pulse voltammetry (DPV), using the following optimized parameters: E_{pulse} = 0.05 V, scan rate =0.003 V s^{-1}, and pulse time =0.07 s. The chronoamperometric response of the (PPV/Pt-SiPy$^+$Cl$^-$)$_6$GOx biosensor to different concentrations of glucose (8.6 x 10^{-5} to 9.8 x 10^{-5} mol L^{-1}) was performed with a μ-Autolab type III potentiostat. Amperometric detection proceeded with constant-potential amperometry, which required preconditioning (~200 s) and operation of the electrode at a constant applied potential ($E_{applied}$ = 1.06 V). When the current reached a baseline in the absence of the substrate, every 50s, glucose was added.

3. RESULTS AND DISCUSSION

3.1 Construction and characterization of LbL films

The Pt-SiPy$^+$Cl$^-$ nanohybrid was well characterized according to a method reported elsewhere [6,10]. Supplementary experiments obtained by DLS measurements were evaluated to provide the size distributions of the Pt-SiPy$^+$Cl$^-$ nanohybrid (Fig. 1). The histogram indicates well-organized PtNPs and good distribution of the PtNPs in the SiPy$^+$Cl$^-$ polymer with a size between 3 and 50 nm, with the majority of PtNPs having an average size of 18.58 nm. These sizes were confirmed with TEM images of the Pt-SiPy$^+$Cl$^-$ [6]. The literature shows similar values of the size of PtNPs, for example Nguye, V. L et al [32] prepared PtNPs (20 nm) by the modified polyol method using silver nitrate as modifying agent. However, comparing the use of SiPy$^+$Cl$^-$ as a nanoreactor, this requires less amount of reagent in relation to polyol method. DLS measurements were also useful for the determination of zeta potential of the Pt-SiPy$^+$Cl$^-$ as nanoreactor.

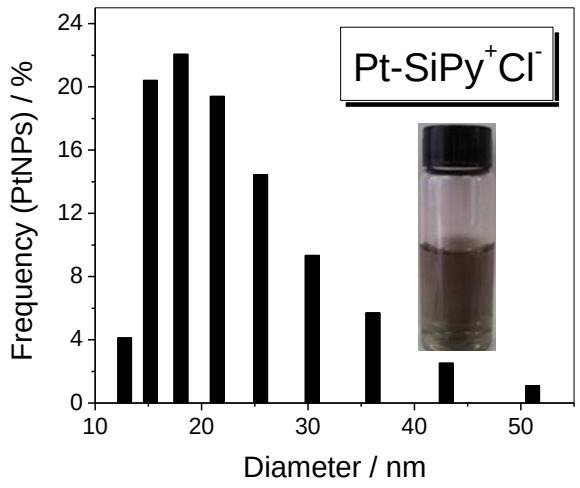

Figure 1. Frequency of size distributions of Pt-SiPy$^+$Cl$^-$. *Inset*: Image of the Pt-SiPy$^+$Cl$^-$ solution.

The value found (173.33 mV) to zeta potential suggests the presence of positively charged groups in the structure of Pt- $SiPy^+Cl^-$, which demonstrate the possibility of using this hybrid as polycation to form LbL films.

Multilayer films growth on quartz slides was monitored by UV-Vis absorption spectroscopy. Initially, the spectra of precursors were carried out to further compare with LbL films. The PPV-SO_3 2.0 mmol L^{-1} solution spectrum exhibits absorption bands at 295, 368 and 428 nm, which corresponds to the $\pi \rightarrow \pi^*$longitudinal transitions of the PPV-SO_3backbones [33] (Fig. 2a). The broad absorption band at 368 nm corresponds to the pendant groups of sulphur trioxide [35,34] and transversal transitions of delocalized states of rigid backbones [35]. The Pt-$SiPy^+Cl^-$ nanohybrid spectrum exhibits an absorption band at 255 nm, which is attributed to the $\pi \rightarrow \pi^*$ transition of the pyridine groups in $SiPy^+Cl^-$ [6,7]. As can be observed in the spectra of the Fig. 2a, the (PPV/ Pt-$SiPy^+Cl^-)_n$ and (Pt-$SiPy^+Cl^-$/PPV)$_n$ LbL films showed the bands at 259, 297, 363 and 428 nm and 259, 297, 363 and 428 nm, respectively attributed to $\pi \rightarrow \pi^*$ transition of the pyridine groups in $SiPy^+Cl^-$**Error! Bookmark not defined.**, $\pi \rightarrow \pi^*$ longitudinal transitions of the PPV-SO_3 backbones [35], pendant groups of sulphur trioxide and transversal transitions of delocalized states of rigid backbones [35] and $\pi \rightarrow \pi^*$ longitudinal transitions of the PPV-SO_3 backbones [35]. It is possible to observe that there were shifts and reductions in the intensity of the bands of 255 to 259, 295 to 297 and 368 to 363 nm from precursors after the formation of the bilayers on quartz. These shifts are also indicative of the electrostatic interactions between of pyridinium ion of Pt-$SiPy^+Cl^-$ and PPV-SO_3 in the LbL film. In similar study, the interaction between sulphonic groups of sulphonated copper phthalocyanine with pyridinium ion of $SiPy^+Cl^-$ was confirmed XPS measurements of the ($SiPy^+Cl^-$/CuTsPc)$_n$ LbL film [3]. Furthermore, the steady linear increase in absorbance intensities at 297nm with a number of deposited layers (n = 3 - 30) indicates progressive LbL assembly growth with R = 0.997 and R = 0.994 for the architectures of (PPV/Pt-$SiPy^+Cl^-)_n$ and (Pt-$SiPy^+Cl^-$/PPV)$_n$, respectively (Fig. 2b). This indicates that the same quantity of precursors of Pt-$SiPy^+Cl^-$ and PPV-SO_3 is adsorbed during each deposition step. However, it was found that for the (PPV/Pt-$SiPy^+Cl^-)_n$ architecture there was a greater absorbance at each bilayer deposited, which can probably be associated to better organization of the species in this architecture (Fig. 2c). The adsorption kinetics of polyelectrolytes was performed by varying the immersion time (10 - 600 seconds) of the quartz substrate in PPV-SO_3 and Pt-$SiPy^+Cl^-$ solutions. By analyse of Fig. 2d, it is apparent that the deposition of the species on the substrate surface had a linear growth between 10 and 60 seconds (R = 0.999).

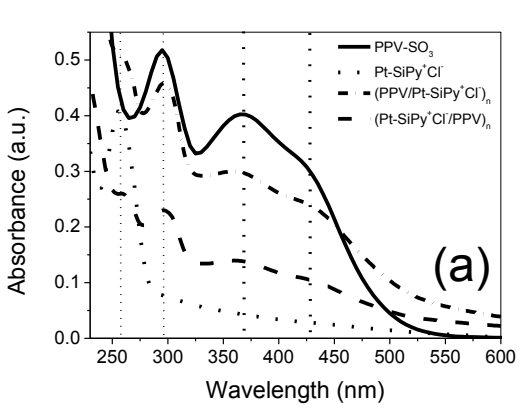

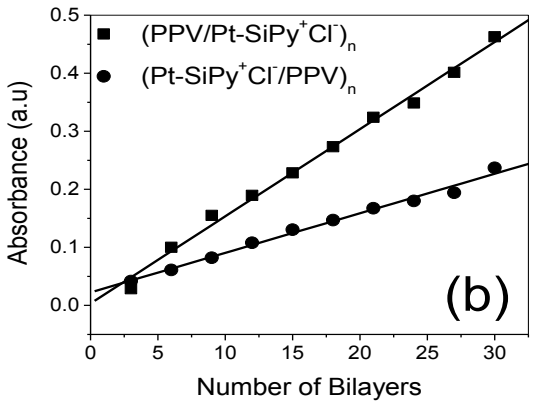

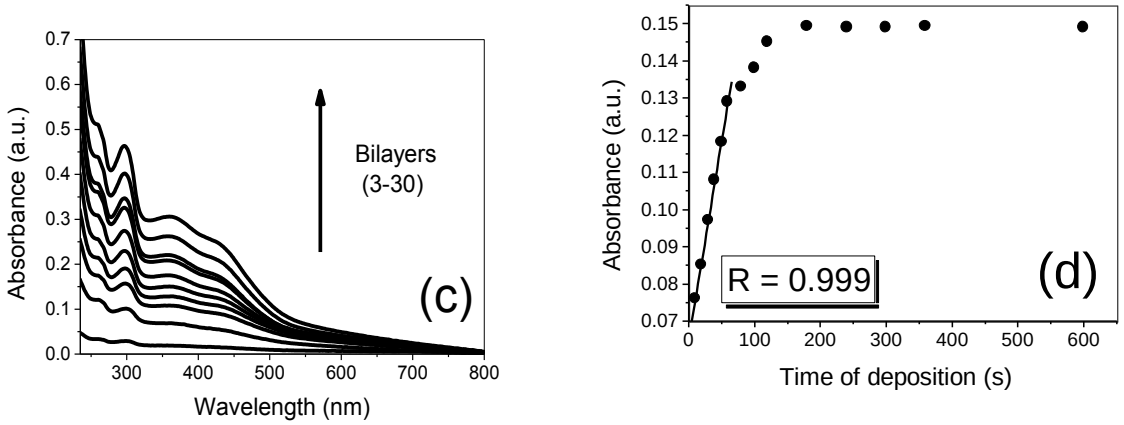

Figure 2. (a) UV-Vis spectra of Pt-$SiPy^+Cl^-$, PPV-SO_3 2mmol L^{-1}, $(PPV/Pt\text{-}SiPy^+Cl^-)_{30}$ and $(Pt\text{-}SiPy^+Cl^-/PPV)_{30}$ LbL films; **(b)** Relationship between the absorbance of 297 nm band as a function of the number of bilayers; **(c)** UV-Vis spectra of the $(PPV/Pt\text{-}SiPy^+Cl^-)_n$ LbL film with different bilayers; and **(d)** Adsorption kinetic of the $(PPV/Pt\text{-}SiPy^+Cl^-)_n$ LbL film.

Between 1 and 3 minutes the correlation decreased gradually and the maximum adsorbed species on the substrate surface was then reached. Thus, to ensure a greater number of species presented in the substrate, a minimum immersion time of 3 minutes is necessary.

FTIR spectroscopy measurements were performed in order to confirm the presence of PtNPs in $SiPy^+Cl^-$ and the presence of polyelectrolytes in the LbL films. The spectra obtained were showed in another study where the $(PPV/Pt\text{-}SiPy^+Cl^-)_3$ LbL film was used as a sensor to detection of encapsulated DA into liposomes [10]. The analysis of the spectrum of PPV-SO_3 drop-coated film allows us to observe the bands at 1189 and 1047 cm^{-1} for the symmetric and asymmetric stretching of the (S=O) group, respectively [35]. The $SiPy^+Cl^-$ spectrum shows a band at1103 cm^{-1} for the symmetric stretching group (Si-O-Si) and others in the region between 820 and 980 cm^{-1} attributed to different vibrational modes with large contribution of bands related to angular deformation of the Si-C-H group and stretching of the Si-C bond [6,36,37] of the band of the Si-O-Si symmetric stretching of the network vibration (1045 cm^{-1}). The confirmation of PtNPs in $SiPy^+Cl^-$ is noted with the disappearance of the bands of $SiPy^+Cl^-$ in the region between 820 and 980 cm^{-1} [6]. Furthermore, the presence of PtNPs in $SiPy^+Cl^-$ reduces the intensity of the Si-O-Si band asymmetric stretching of the cage structures (1103 cm^{-1}) [6,38]. The incorporation of PtNPs into $SiPy^+Cl^-$ causes a hindrance of the vibrational modes of the material structure, decreasing the degrees of freedom for the stretching or bending of the Si-O-Si, Si-C-H and Si-C bonds [6]. Although the vibrational modes of the $SiPy^+Cl^-$ backbone are sterically hindered, the Si-O-Si groups near the nanoparticle surface in the cage are almost free to vibrate. This observation explains the fact that only the vibrational mode of the cage structure is active [6].

In addition, the disappearance of most of the bands assigned to the Si skeleton indicates that the interactions between the PtNPs and the $SiPy^+Cl^-$structure have only a steric nature, due to the fact that chemical interaction should provide shifts in the characteristic bands of the matrix, as well as the appearance of new bands, as observed in previous studies [3,6,10,37].

FTIR spectra of the LbL films containing 30 bilayers of $(PPV/Pt\text{-}SiPy^{+}Cl^{-})_{30}$ and $(Pt\text{-}SiPy^{+}Cl^{-}/PPV)_{30}$ confirmed the presence of both PPV-SO_3 and Pt-$SiPy^{+}Cl^{-}$. It can be noted that the spectra of these films indicate primary bands of PPV-SO_3 assigned at asymmetric stretching of the S=O group [37] and primary bands of Pt-$SiPy^{+}Cl^{-}$ at 1108 cm^{-1} attributed to asymmetric stretching of the Si-O-Si group [6,40]. However, it is also noteworthy that S=O stretching of the PPV-SO_3 band is shifted from 1048 and 1187 cm^{-1} in the spectrum of PPV-SO_3 to 1037 and 1203 cm^{-1} in the spectra of the LbL films. These results, combined with UV-Vis spectroscopy, confirm that the shifts occur due to the interaction in the LbL films between the SO_3^{-} groups of the PPV-SO_3 and the pyridine rings of Pt-$SiPy^{+}Cl^{-}$, similar to that observed in other studies involving CuTsPc with $SiPy^{+}Cl^{-}$ [3], PANI with sulphonated phthalocyanine [39] **Error! Bookmark not defined.**, and Pt-PAMAM with PVS [37] based in LbL films.

The spectra in Fig. 3 show the Raman scattering of drop-coated films of $SiPy^{+}Cl^{-}$, Pt-$SiPy^{+}Cl^{-}$, PPV-SO_3 and LbL films of $(PPV/Pt\text{-}SiPy^{+}Cl^{-})_{30}$ deposited onto silver substrates.

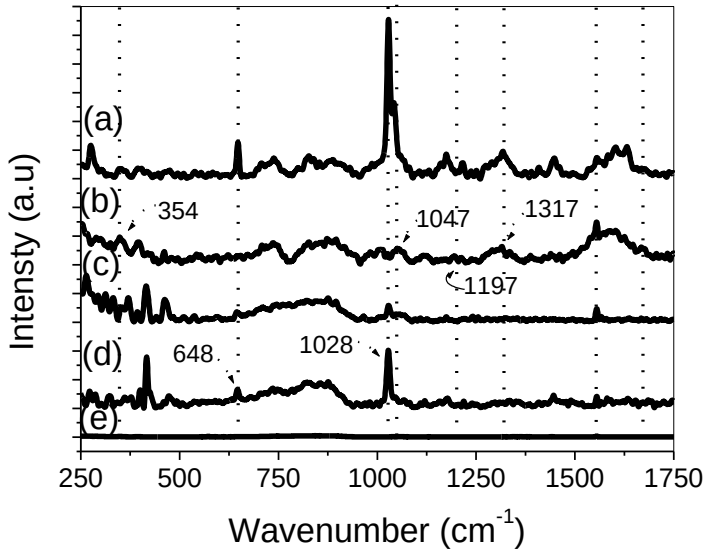

Figure 3. Raman spectra of the films of (a) $(PPV/Pt\text{-}SiPy^{+}Cl^{-})_{30}$ LbL film, (b) drop-coated film of PPV-SO_3, (c) drop-coated film of Pt-$SiPy^{+}Cl^{-}$, (d) drop-coated film of $SiPy^{+}Cl^{-}$, and (e) Ag substrate.

The spectral scattering (Fig. 3) of $SiPy^{+}Cl^{-}$ and Pt-$SiPy^{+}Cl^{-}$ showed bands at 1028 cm^{-1} (strong) and 644 cm^{-1} (medium), respectively, which can be assigned to the breathing mode of the pyridine ring and the deformation in the plane of the ring, respectively [6,40]. The Raman spectra of PPV-SO_3 exhibits bands at 354, 1047, 1197 and 1313 cm^{-1}, which can be assigned to deformation in the plane of the benzene ring, deformation of the C-H group of the ring in the plane, symmetrical stretching of the SO_3^{-}group, and symmetrical C-C stretching of the vinyl group [41,42]. The presence of the polyelectrolytes PPV-SO_3 and Pt-$SiPy^{+}Cl^{-}$ in the LbL films can be verified by the existence of their

characteristic bands of these polyelectrolytes in the spectra of the $(PPV/Pt\text{-}SiPy^{+}Cl^{-})_{30}$ LbL film and for the shifts related the interactions between the precursors.

3.2 Morphological Characterization

AFM images for the films $(PPV/Pt\text{-}SiPy^{+}Cl^{-})_{n}$ (n = 5, 10, 15 and 20) (Fig. 4a-d), revealed an average roughness of the film that is listed in Table 1. An increase can be observed in the roughness of the film containing 5 bilayers (11,371nm) until 20 bilayers (14,769nm) of $(PPV/Pt\text{-}SiPy^{+}Cl^{-})_{n}$.

Table 1. Root-mean-square (RMS) roughness for $(PPV/Pt\text{-}SiPy^{+}Cl^{-})_{n}$ and $(Pt\text{-}SiPy^{+}Cl^{-}/PPV)_{5}$ LbL films.

Number of bilayers	RMS roughness (nm) (5 × 5 μm)
$(PPV/Pt\text{-}SiPy^{+}Cl^{-})_{5}$	11.371
$(PPV/Pt\text{-}SiPy^{+}Cl^{-})_{10}$	12.662
$(PPV/Pt\text{-}SiPy^{+}Cl^{-})_{15}$	13.177
$(PPV/Pt\text{-}SiPy^{+}Cl^{-})_{20}$	14.769
$(Pt\text{-}SiPy^{+}Cl^{-}/PPV)_{5}$	11.437

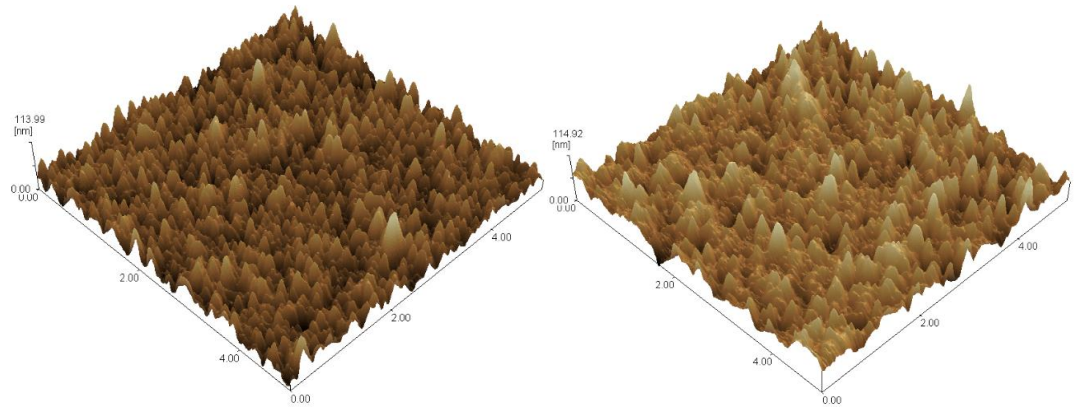

(a) (b)

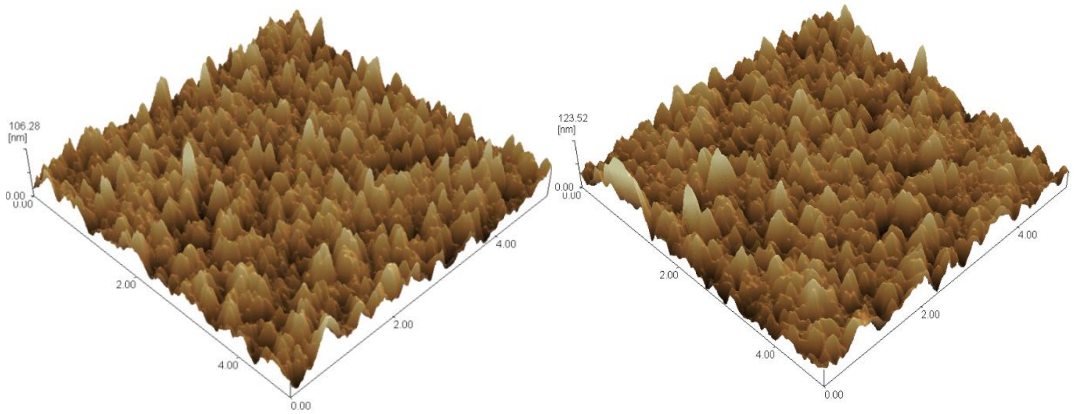

(c) (d)

Figure 4. AFM images of (a) (PPV/Pt-$SiPy^+Cl^-$)$_5$, (b) (PPV/Pt-$SiPy^+Cl^-$)$_{10}$, (c) (PPV/Pt-$SiPy^+Cl^-$)$_{15}$, and (d) (Pt-$SiPy^+Cl^-$/PPV)$_{20}$ LbL films.

It is important to note that during the deposition of the first bilayers, the molecules are deposited randomly until the entire substrate is covered, decreasing the roughness. This can be seen by comparing the roughness of the surface of the FTO substrate (14.859 nm) with the roughness of the LbL films. Since the layers are deposited, the adsorbed molecules and non-adsorbed chains are expected to aggregate, which causes an increase in the roughness and in the size of the grains with the increase in the number of bilayers (5 to 20 bilayers). Similar results have been obtained for others LbL film containing $SiPy^+Cl^-$, such as $SiPy^+Cl^-$/CuTsPc [3] and PVS/Pt-$SiPy^+Cl^-$ [6]. The growth in the thickness of the LbL films is linear from 5 to 20 bilayers. The (Pt-$SiPy^+Cl^-$/PPV)$_n$ (n = 5 to 20 bilayers) LbL films showed the same behaviour (results not shown).

3.3 Electrochemical detection of H_2O_2 with LbL films

Initially the different architectures of LbL films of (PPV/Pt-$SiPy^+Cl^-$)$_6$ and (Pt-$SiPy^+Cl^-$/PPV)$_6$ were studied by cyclic voltammetry to evaluate the sensing properties of LbL films in the presence of H_2O_2. The aim of H_2O_2 detection is due to the fact that this analyte is generated in the proportion of 1:1 in the enzymatic reaction between glucose and the enzyme GOx [21]. In addition, H_2O_2 detection is important because this oxidant is used in bleaching processes in the textile, cellulose and paper industries [43]. Furthermore, in the medical field, their presence should be monitored to prevent cells from undergoing stress [44].

Fig. 5a depicts the cyclic voltammogram for H_2O_2 oxidation recorded at FTO, (PPV/Pt-$SiPy^+Cl^-$)$_6$ and (Pt-$SiPy^+Cl^-$/PPV)$_6$ in an electrolyte solution of PBS (0.1 mol L^{-1}, pH 7) at a scan rate of 30 mVs^{-1} at a fixed concentration of H_2O_2 1.0 x 10^{-4}mol L^{-1}. Comparing the results obtained from the (PPV/Pt-$SiPy^+Cl^-$)$_6$ and (Pt-$SiPy^+Cl^-$/PPV)$_6$LbL films with FTO, it can be observed that the LbL films provided higher values of oxidation current than the observed to FTO electrode with Ipa = 6.16 and 5.15 μA for the (PPV/Pt-$SiPy^+Cl^-$)$_6$ and (Pt-$SiPy^+Cl^-$/PPV)$_6$ LbL films respectively, against Ipa = 2.07 μA for the FTO electrode. In addition, the (PPV/Pt-$SiPy^+Cl^-$)$_6$ with the PtNPs on the outer surface of the electrode showed a more negative potential than the observed to FTO electrode. This observation shows the viability and importance of the modification of the FTO surface with PPV-SO_3 and Pt-$SiPy^+Cl^-$ polyelectrolytes. Furthermore, as can be seen in Fig. 5a, in terms of current response, (PPV/Pt-$SiPy^+Cl^-$)$_6$LbL film shows higher favourable electrochemical activity towards the catalysis of H_2O_2 than (Pt-$SiPy^+Cl^-$/PPV)$_6$, suggesting that PtNPs on the outer surface of the electrode promote the catalytic oxidation of H_2O_2. The literature shows the importance of the presence of metal nanoparticles on the electrode surface due to their small size (1–100 nm), unique chemical, physical and electronic properties (different from bulk material), flexibility to construct novel and improved sensing devices [13,45,46]. The performance of the (PPV/Pt-$SiPy^+Cl^-$)$_6$ LbL film in the H_2O_2 oxidation can be attributed to presence of PtNps in the surface of the electrode because when the electrochemical behaviour of the electrode is compared with the obtained with the (PPV/$SiPy^+Cl^-$)$_6$LbL film without PtNPs is not verified the redox process of the H_2O_2 (Fig. 5c).

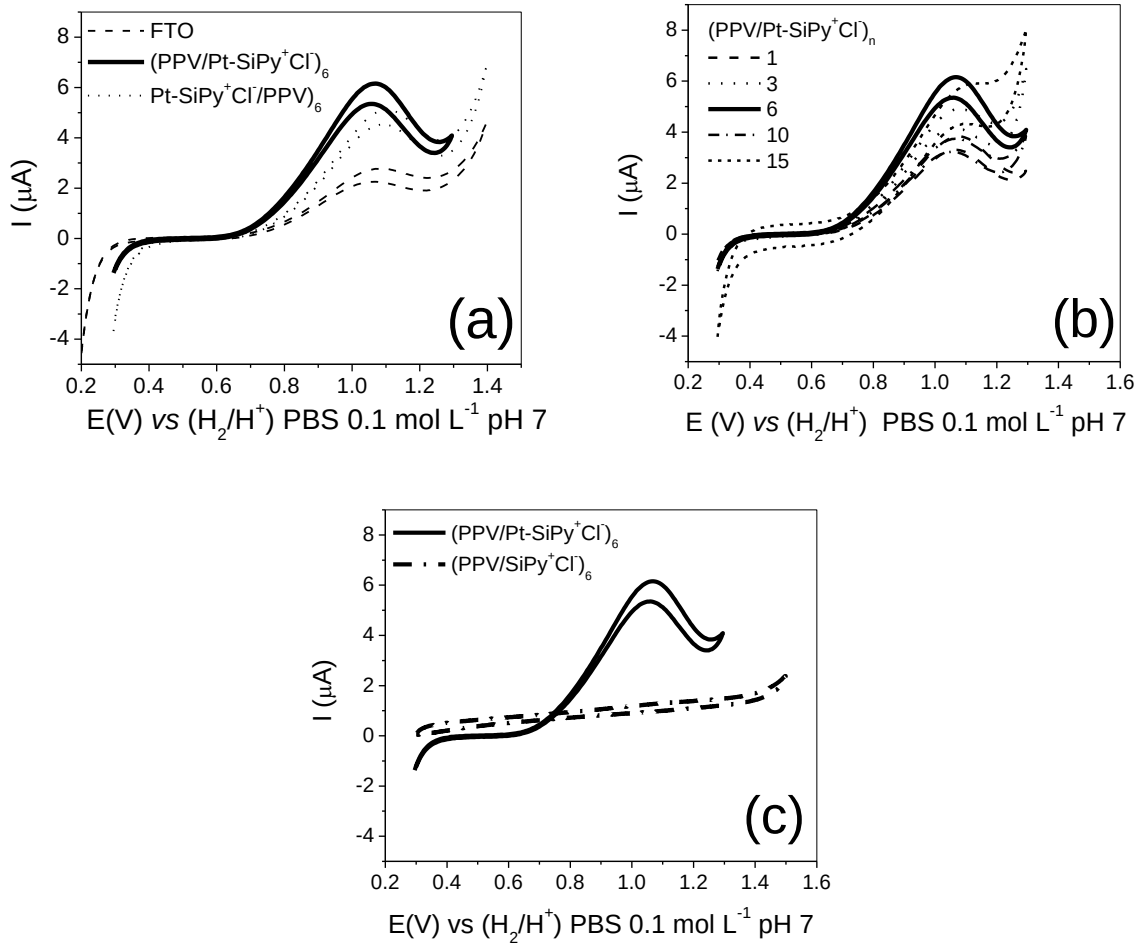

Figure 5. Cyclic voltammograms of **(a)**FTO, $(PPV/Pt\text{-}SiPy^{+}Cl^{-})_6$ and $(Pt\text{-}SiPy^{+}Cl^{-}/PPV)_6$ LbL films; **(b)** $(PPV/Pt\text{-}SiPy^{+}Cl^{-})_n$ LbL films with *n* bilayers and (c) $(PPV/Pt\text{-}SiPy^{+}Cl^{-})_6$ and $(PPV/SiPy^{+}Cl^{-})_6$ LbL films. All measurements were performed in $[H_2O_2] = 1.0 \times 10^{-4}$ mol L^{-1} in 0.1 mol L^{-1} PBS (pH 7) at 30 mVs^{-1}.

As showed in Fig. 5b, it was noted that $(PPV/Pt\text{-}SiPy^{+}Cl^{-})_6$ LbL films provided higher values of oxidation current for H_2O_2 than the same platform containing others bilayers (n = 1, 3, 10 and 15 bilayers), due to the film resistance that occurs with an increase in the number of bilayers. The same number of bilayers was found by Wu et al. for glucose biosensor based in layer-by-layer assembled chitosan/gold nanoparticles/glucose oxidase modified Pt electrode. In this work was observed that the electrode reached saturation after the seven layers [29].

In the study by Tsai, M. C and Tsai, Y. C [30], it was observed that the improvement in electrocatalytic activity of H_2O_2 at the platinum-multiwalled carbon nanotube alumina-coated silica (Pt-MWCNT-ACS) nanocomposite modified electrode is due the incorporation of PtNPs within the MWCNT-ACS matrix. The influence of the PtNPs combined with MWCNT in the electrochemical activity was analyzed and it was verified that the presence of the PtNPs in the electrode it was crucial to the H_2O_2 redox process because without the PtNPs the same process is not observed. Similar

behaviour was observed for dopamine (DA) oxidation in another study with (PVS/Pt-SiPy^{+}Cl^{-})$_3$ LbL film [6] that exhibited excellent response for the detection of DA in the presence of ascorbic acid interferent. This response was attributed to the presence of PtNPs on the surface of the LbL film [6].

The relationship between the oxidation current (Ipa) and the square root of the scan rate ($\nu^{1/2}$) in the presence of H_2O_2 1.0 x 10^{-4} mol L^{-1} (Fig. 6a), shows that the redox process of H_2O_2 obtained with the (PPV/Pt-SiPy^{+}Cl^{-})$_6$ LbL film is controlled by diffusion [47,48]. Furthermore, it was found that the (PPV/Pt-SiPy^{+}Cl^{-})$_6$ electrode provided a decrease in the overpotential of activation of H_2O_2, which agrees with the correlation of Nicholson Shain [49] suggesting a process for electron transfer assisted by the presence of PPV-SO_3 and Pt-SiPy^{+}Cl^{-} polyelectrolytes on FTO, as shown in Fig. 6b.

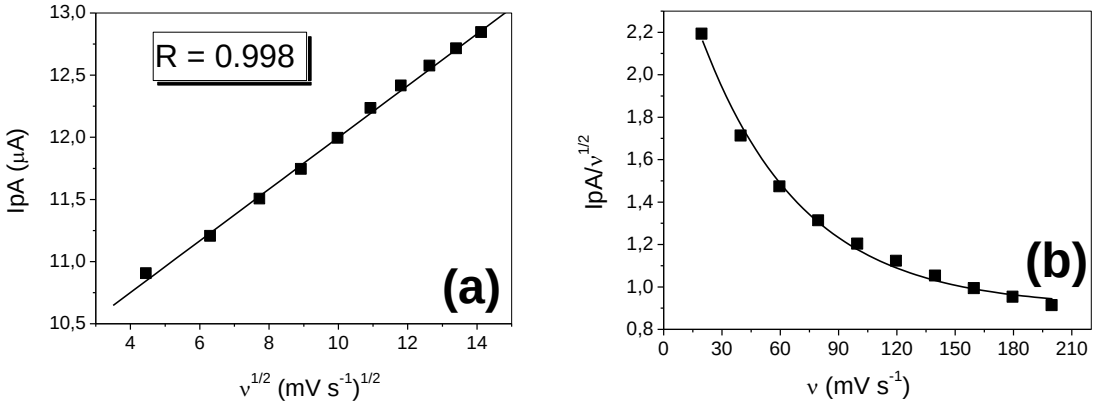

Figure 6. Relationship between **(a)** Ipa and the square root of scan rate ($\nu^{1/2}$), and **(b)** Ipa/$\nu^{1/2}$ as a function of scan rate of the modified electrode (PPV/Pt-SiPy^{+}Cl^{-})$_6$, in H_2O_2 1.0 x 10^{-4} mol L^{-1} in 0.1 mol L^{-1} PBS (pH 7) at 30 mVs^{-1}.

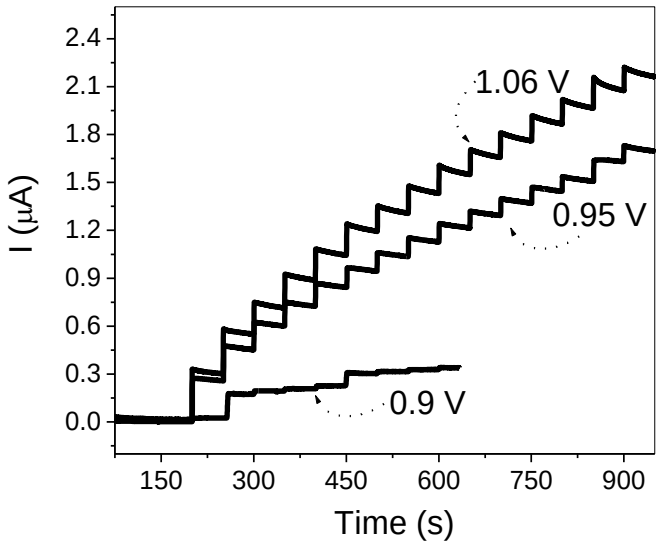

Figure 7. Amperometric response obtained at different potentials performed in PBS 0.1 mol L^{-1}, pH 7 with a 6-bilayers of (PPV/Pt-SiPy^{+}Cl^{-}) LbL film deposited onto FTO in the presence of different concentrations of H_2O_2 (addition time of 50 s). (1,0 x 10^{-5} – 1,3 x 10^{-4} mol L^{-1}).

After the choice of the electrode, electrochemical studies were performed in order to check the best potential to oxidize H_2O_2 on the electrode surface of the (PPV/Pt-SiPy$^+$Cl$^-$)$_6$ LbL film. For these measurements, a stock solution of 1.0 x 10^{-4} mol L^{-1} H_2O_2 was used with successive additions of 50 µL at 50 seconds. Thus, chronoamperometry measurements were made at fixed potentials of 0.9, 0.95 and 1.06 V with the LbL film. As can be observed in Fig. 7, these results revealed that by applying a potential of 1.06 V, the (PPV/Pt-SiPy$^+$Cl$^-$)$_6$ LbL film shows higher sensitivity (R = 0.998) in the process of detection of H_2O_2.

3.4 Detection of glucose on the (PPV/Pt-SiPy$^+$Cl$^-$)$_6$GOx LbL film

After verifying the possibility of detecting of H_2O_2 with the (PPV/Pt-SiPy$^+$Cl$^-$)$_6$ LbL film, the modification of the electrode with GOx was performed. The aim was to quantify glucose by indirectly detecting the H_2O_2 generated in the reaction that occurs at the surface of the enzymatic electrode. The fact that the proportion of glucose to H_2O_2 generated in the reaction is 1:1 enables the indirect determination of glucose for the oxidation reaction of H_2O_2on the electrode surface [50,51]. Thus, the 2 mg mL^{-1} GOx solution was immobilized by LbL technique on the surface of the (PPV/Pt-SiPy$^+$Cl$^-$)$_6$ film in order to obtain the (PPV/Pt-SiPy$^+$Cl$^-$)$_6$GOx biosensor.

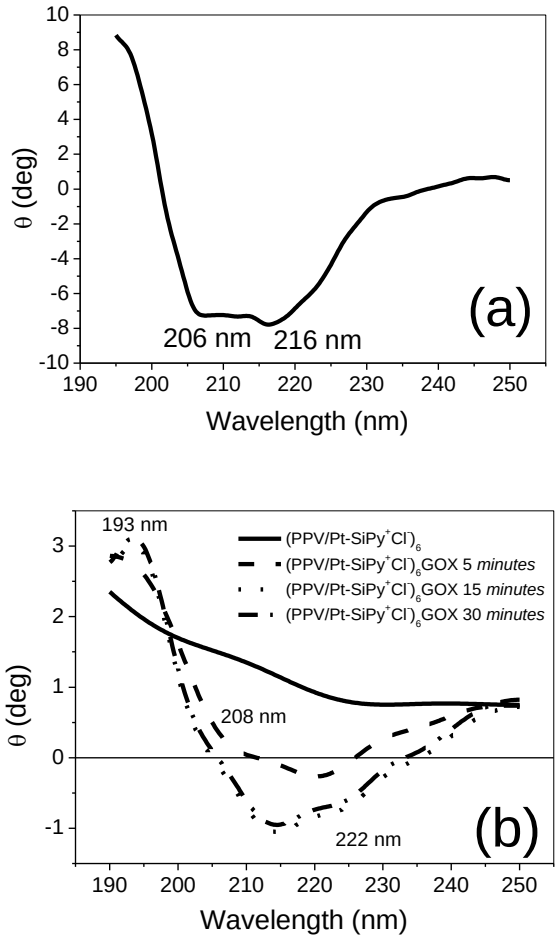

Figure 8. CD spectra of **(a)** 2 mg mL^{-1} GOx solution in 0.1 mol L^{-1} PBS, pH 7; **(b)** (PPV/Pt-SiPy$^+$Cl$^-$)$_6$ and (PPV/Pt-SiPy$^+$Cl$^-$)$_6$GOx LbL films, on quartz substrate.

As observed by M. Ferreira et al [27], the advantage of the LbL method lies on the possibility of minimizing protein denaturing because the adsorption process is carried out in aqueous solutions, under mild conditions. The enzymatic concentration used and the immobilization time were determined based on values found in the literature [19,21]. In conditions where the GOx solution was prepared, the enzyme is negatively charged, this shows that addition to of secondary interactions there are electrostatic interactions between the enzyme and the outer positive surface of $(PPV/Pt\text{-}SiPy^{+}Cl^{-})_6$ LbL film.

In order to verify the maintenance of the α-helix conformational structure of the GOx immobilized on the surface of $(PPV/Pt\text{-}SiPy^{+}Cl^{-})_6$GOx LbL films, circular dichroism measurements using a 2 mg mL^{-1} GOx solution in 0.1 mol L^{-1} PBS (pH 7) were performed (Fig. 8a). The CD spectrum of the α-helix structure has three characteristic transitions in the region (190 - 250 nm) corresponding to n → π * and π → π * electronic transitions [52], with a strong (193 nm) and a weak (206 nm) occurring respectively perpendicular and parallel to the propeller shaft that is assigned to the transition π → π * and yet another parallel to the shaft assigned to the n → π * transition (216 nm) [53]. These characteristic transitions in the spectrum of the α-helical structure were observed in the spectrum of the examined GOx solution (Fig. 8a). This proves the conformational stability of the enzyme solution prepared under conditions of immobilization [54,55].

The enzymatic deposition onto $(PPV/Pt\text{-}SiPy^{+}Cl^{-})_6$ was performed on the last layer in according to related works [16,54,59] due to the fact that the amount of enzyme deposited is sufficient for the enzymatic reaction that occurs in the electrode-solution interface. This method is different from that the enzyme is used as a polyanion and then is placed between the layers to increase the amount of enzyme on the electrode surface [19,21,27]. However, in this study the amount of enzyme deposited on the last layer was sufficient for electrocatalyzing the enzymatic reaction. In enzymatic deposition, the immersion time is important parameter. So, the immersions of GOx were made at 5, 15 and 30 minutes to verify the relationship between immersion time and structural maintenance. The spectra of the $(PPV/Pt\text{-}SiPy^{+}Cl^{-})_6$GOx LbL films prepared at different immersion times (Fig. 8b) present characteristic absorption bands for α-helix conformation. As can be showed the major absorbance is evident for transitions in the LbL films immersed at 15 (212 and 223 nm) and 30 minutes (213 and 223 nm) in the GOx solution in relation to 5 minutes (208 and 220 nm). This indicates that a greater amount of enzyme is available on the surface of the LbL films. However, no significant difference was observed in absorbance with times of 15 and 30 minutes of immersion. Therefore, to ensure a greater amount of GOx on the surface of the films, a time of 30 minutes was selected for preparation of the biosensor. Furthermore, in this time the occurrence of displacements of the absorption bands of the spectrum of the GOx solution is evident in relation to GOx immobilized on the LbL film (206 to 213nm, and 216 to 223 nm, respectively). This can be attributed to interactions between the surface of the film and the GOx enzyme. Under the conditions in which the GOx solution was prepared, the enzyme is negatively charged, which shows that in addition to the presence of helical elements of secondary interactions there are electrostatic interactions between the GOx enzyme and the positive outer surface of the LbL film. These results show the efficiency of the process of enzymatic immobilization, maintaining the secondary structure of the GOx. Similar behaviour was observed by

shifted of bands of the pure enzyme compared with CD spectrum of GOx adsorbed on the surface of the ZnO nanoparticles [55].

The (PPV/Pt-SiPy$^+$Cl$^-$)$_6$GOx LbL film was measured in a fixed concentration of 9.0 x 10^{-5} mol L^{-1} of glucose to verify the potential application of the film as a enzymatic biosensor. As can be seen in Fig. 9a, the cyclic voltammogram obtained with the (PPV/Pt-SiPy$^+$Cl$^-$)$_6$GOx film in the presence of glucose show the profile of the redox process of H_2O_2. This result prove the enzymatic efficient of the GOx immobilized on the electrode surface and confirms the capability of the LbL film to act as a biosensor for glucose. In addition, the (PPV/Pt-SiPy$^+$Cl$^-$)$_6$ without GOx, no showed electrochemical answer to glucose oxidation (Fig. 9a). This results show us the importance of the GOx immobilization on LbL film surface.

The amperometric response of the (PPV/Pt-SiPy$^+$Cl$^-$)$_6$GOx film (Fig. 9b), applying a potential of 1.06 V were performed in the presence of different concentrations of glucose (8.6 x 10^{-5} to 9.8 x 10^{-5} mol L^{-1}). It can be observed, the anodic peak current as a function of H_2O_2 concentration generated in the reaction between GOx and glucose was obtained (inset of Fig. 9b). The analytical parameters obtained from the calibration curve calculated according to IUPAC were: sensitivity of 1.17 μA/mmol L^{-1} cm^{-2}, DL of 27.4 μmoL^{-1} and quantification limit (QL) of 91.4 μmol L^{-1}. According to the latest review about some example of the main nanoparticles-based biosensors for glucose detection realized in the last 10 years reported by V. Scognamiglio [13], the (PPV/Pt-SiPy$^+$Cl$^-$)$_6$GOx biosensor present similar LD. The low value of DL found for this biosensor can be attributed to the large amount of PtNP immobilized by LbL technique and the high surface area of the unique nanostructures formed through the synthetic route. Furthermore, this value demonstrates that detection range is sufficient to be medically useful for example in the monitoring of human blood glucose level, which in normal human range from 4.4 to 6.6 mM [56].

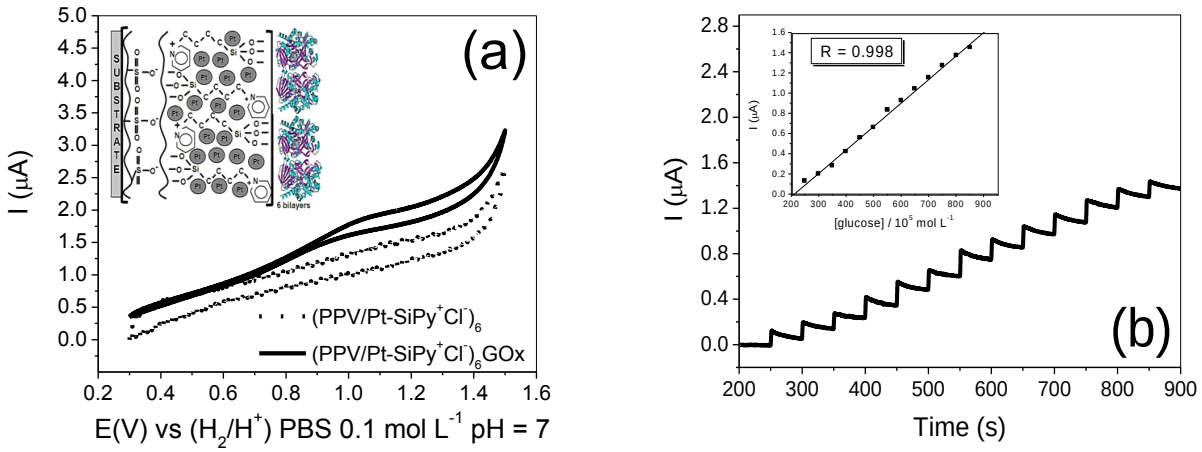

Figure 9. (a) Cyclic voltammogram of (PPV/Pt-SiPy$^+$Cl$^-$)$_6$ and (PPV/Pt-SiPy$^+$Cl$^-$)$_6$GOx in the presence of glucose 9 x 10^{-5} mol L^{-1}, ν = 50 mV s^{-1}. *Inset:* Idealized structure of the LbL structure of alternating PPV-SO$_3$ and Pt-SiPy$^+$Cl$^-$ layers and GOx to result the (PPV/Pt-SiPy$^+$Cl$^-$)$_6$GOx film; and **(b)** Chronoamperometry of the (PPV/Pt-SiPy$^+$Cl$^-$)$_6$GOx LbL film in the presence of different concentrations of glucose at a fixed potential of 1.06 V. *Inset*: calibration curve of the(PPV/Pt-SiPy$^+$Cl$^-$)$_6$GOx film biosensor. Both measurements were performed in PBS 0.1 mol L^{-1}, pH 7.

It was also performed the evaluation of the amperometric response for the film (PPV/Pt-$SiPy^+Cl^-)_6$ for the glucose oxidation without the incorporation of the GOx. It was verified that on this configuration the electrode produce no oxidation current despite the Glucose concentration (see Figure 9 (a)). This results indicated that the good current response obtained for the configuration (PPV/Pt-$SiPy^+Cl^-)_6$GOx must be assigned to the GOx presence.

The apparent Michaelis-Menten constant (k_m^{app}), an indicator of enzyme-substrate reaction kinetics, was used to evaluate the biological activity of the immobilized enzyme. k_m^{app} can be calculated using the Lineweaver-Burk equation (1) [57]:

$$\frac{1}{I_{ss}} = \frac{1}{I_{\max}} + \frac{k_m^{app}}{I_{\max} C_{glucose}} \qquad [1]$$

where $\boldsymbol{I_{ss}}$ is the steady-state response current after the addition of the substrate, $\boldsymbol{I_{max}}$ is the maximum current under saturated substrate conditions, and $\boldsymbol{C_{glucose}}$ is the bulk concentration of glucose. Thus, in order to determine the enzymatic kinetics of the GOx immobilized in the (PPV/Pt-$SiPy^+Cl^-)_6$GOx LbL film, chronoamperometry measurements were performed adding aliquots of 50 μL^{-1} of a stock solution of glucose 10^{-3} mol L^{-1} into a 10mL electrochemical cell to verify the saturation of the active sites of GOx by the disappearance of the signal of oxidation current of the H_2O_2 formed in the enzymatic reaction (Fig. 10a). From the current values of oxidation, the graph of double reciprocal or Lineweaver and Burk (Fig. 10b) was obtained. From this graph, k_m^{app} was determined as being equal to 2.64 mmol L^{-1}, which is similar to values found in the literature [14,58]. This value represents the concentration of glucose needed to reach half of the maximum oxidation current.

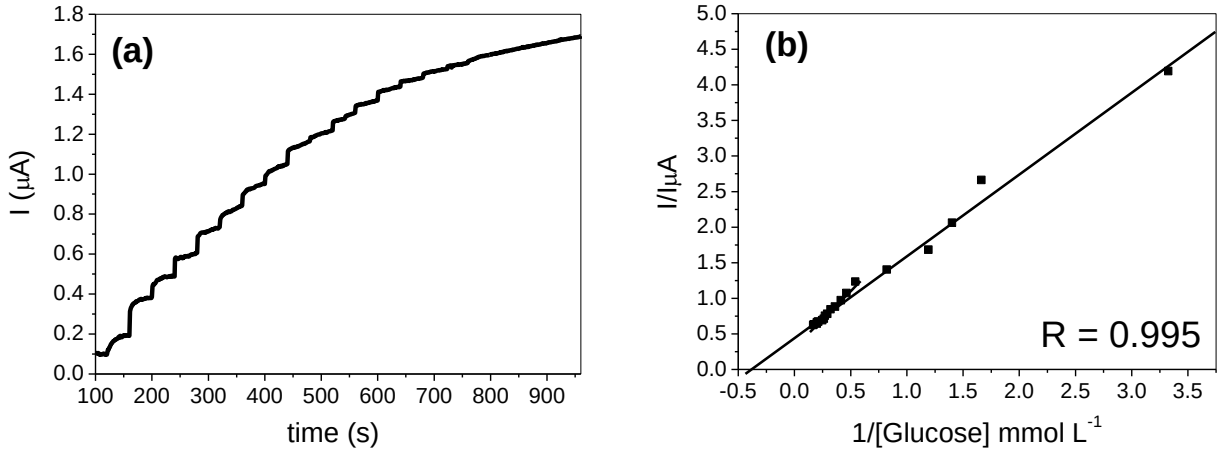

Figure 10. (a) Chronoamperometry of the (PPV/Pt-$SiPy^+Cl^-)_6$GOxLbL film in different concentrations of glucose (addition of aliquots of 50 μL^{-1} of a stock solution of glucose 10^{-3} mol L^{-1}); and **(b)** Double reciprocal or Lineweaver and Burk, obtained with the (PPV/Pt-$SiPy^+Cl^-)_6$GOx LbL film (E = 1.06 V, at 50 s). Both measurements were performed in PBS 0.1 mol L^{-1}, pH 7.

Comparing the performance of the (PPV/Pt-SiPy$^+$Cl$^-$)$_6$GOx biosensor with another found in the literature emphasis can be given to the low detection limit (DL) (27.4 μmol L^{-1}). Most biosensors in the literature that exhibit low DL values are those with mediators in the constitution [16,18,20]. The low value of DL found for this biosensor can be attributed to the presence of PtNPs in the films, which increase the process of electron transfer at the electrode surface. However, although any biosensors as the GOx/Pt/OMC/Au where OMC means mesoporous carbon shows a lower sensitivity (0.38 μA/mmol L^{-1} cm^{-2}) than obtained with the (PPV/Pt-SiPy$^+$Cl$^-$)$_6$GOx (1.17 μA/mmol L^{-1} cm^{-2}), the preparation process is more complex, because it requires a larger amount of reagents and a longer time of preparation [14].

The value to sensitivity from the (PPV/Pt-SiPy$^+$Cl$^-$)$_6$GOx is similar to that obtained by Mattos et al [59], but the LbL method offers two advantages: an efficient enzyme immobilization due to the mild conditions used and a smaller amount of enzyme in comparison with the cross-linking methods. Moreover, the LbL method allows fine thickness control of the enzymatic layer to avoid mass transport problems [27].

In addition, it is important to note that the LbL method of immobilization of PtNPs on solid platform FTO is efficient, showing that the PtNPs ~~if~~ remained stable and exerted fundamental role in the oxidation of the H_2O_2 generated in the enzymatic reaction. Different kind of NPs can be obtained as the prepared by Li et al [60], that studied the amino group modified mesoporous silica NPs (MSN) which were used to immobilize PtNPs and GOx, demonstrating high stability and reactivity for catalyzing H_2O_2 electro-reduction, due to the large amount of PtNPs immobilized and the high surface area of the unique nanostructures formed through the synthetic route. However, this method is harder due to higher complexity of the synthetic route compared with the LbL method considered a simple and of low cost.

4. CONCLUSIONS

The nanohybrid Pt-SiPy$^+$Cl$^-$ was found to be an efficient enzymatic stabilizer of GOx. The presence of PtNPs on the outer surface of the (PPV/Pt-SiPy$^+$Cl$^-$)$_6$GOx electrode was essential for detection because they assist the redox process of H_2O_2 formed in the enzymatic reaction. The PPV-SO_3 polyelectrolyte proved to be efficient as a polyanion in the process of construction of biosensors by the LbL technique. It was found by CD measurements that the GOx enzyme retains its conformational structure when it is immobilized. This indicates the efficiency of the immobilization process of the LbL technique. This maintenance of the surface structure of the films explains the excellent enzymatic activity of GOx measured by k_m^{app} = 2.64 mmol L^{-1}. Analytical performance of the (PPV/Pt-SiPy$^+$Cl$^-$)$_6$GOx biosensor showed a linear response to glucose detection in a wide range between 8,6 x 10^{-5} to 9,8 x 10^{-5} mol L^{-1}, in addition to a stability of 30 days. These results demonstrated that the novel nanocomposite PPV/Pt-SiPy$^+$Cl$^-$ provided high accessibility to electrons between the enzyme and the electrode, improving electrocatalytic behaviour. Parameters such as the

low DL and low QL obtained with the biosensor showed the high capacity and efficiency of this nanocomposite for detection of H_2O_2 in enzymatic reactions where this analyte is directly involved.

ACKNOWLEDGMENTS
The authors wish to thank CNPq, INEO/INCT/CNPq and nBioNet/CAPES (Brazil) for their financial support of this work.

References

1. L. A. Soares, T. F. S. Da Silveira, D. R. Silvestrini, U. O. Bicalho, N. L. Dias Filho and D. R. Do Carmo, *Int. J. Electrochem. Sci.,* 8 (2013) 4654.
2. C. G. Jesus, C. M. S. Forte, K. Wohnrath, C. A. Pessoa, J. E. S. Soares, S. T. Fujiwara, P. L. Neto and A. N. Correia, *Electroanalysis*, 23 (2011) 1814.
3. C. G. Jesus, V. Dos Santos, C. D. Canestraro, V. Zucolotto, S. T. Fujiwara, Y. Gushikem, K. Wohnrath and C. A. Pessoa, *J. Nanosci. Nanotechonol.*, 11 (2011) 3499.
4. S. W. Kuo and F. C. Chang, *Prog. Polym .Sci.*, 36 (2011) 1649.
5. D. B. Cordes, P. D. Lickiss and F. Rataboul, *Chem. Rev.*, 110 (2010) 2081.
6. V. dos Santos, C. G. Jesus, M. Dos Santos, C. D. Canestraro, V. Zucolotto, S. T. Fujiwara, J. R. Garcia, C. A. Pessoa and K. Wohnrath, *J. of Nanoparticles Res.* 14 (2012) 1081.
7. S. T. Fujiwara, Y. Gushikem and R. V. S. Alfaya, *Colloids Surf. A: Physicochem.and Engineering Aspects*, 178 (2001) 135.
8. A. A. Muxel, D. A. De Jesús, R. V. S. Alfaya and A. A. S. Alfaya, *J. Braz. Chem. Soc.*, 18 (2007) 572.
9. S. T. Fujiwara, C. A. Pessoa and Y. Gushikem, *Electrochim. Acta*, 48 (2003) 3625.
10. V. Dos Santos, M. Dos Santos, B. Sandrino, C. G. Jesus, J. R. Garcia, S. T. Fujiwara, C. A. Pessôa, and K. Wonhrath, *ECS Trans.,* 50 (2013)43.
11. E. W. De Menezes, M. R. Nunes, L. T. Arenas, S. L. P. Dias, I. T. S. Garcia, Y. Gushikem, T. M. H. Costa and E. V. Benvenutti, *J Solid State Electrochem*, 16 (2012) 3703.
12. N. Cheng, H. Wang, X. Li and L. Zhu, *Am. J. of Anal. Chem.*, 3 (2012) 312.
13. V. Scognamiglio, *Biosens. and Bioelectron.*, 47 (2013) 12.
14. W. Li, R. Yuan, Y. Chai, H. Zhong and Y. Wang, *Electrochimica. Acta*, 56 (2011) 4203.
15. H. Wang, C. Zhou, J. Liang, H. Yu and F. Peng, *Int. J. Electrochem. Sci.,* 3 (2008) 1180.
16. D. Liu, H. Liu and N. Hu, *Electrochim. Acta*, 55 (2010) 6426.
17. J. F. Rusling, E. G. Hvastkovs, D. O. Hulla and J. B. Schenkman, *Chem. Commun.*, 141 (2008) 141.
18. B. Yin, R. Yuan, Y. Chai, S. Chen, S. Cao, Y. Xu and P. Fu, *BiotechnolLett*, 30 (2008) 317.
19. Q. Gao, Y. Guo, J. Liu, X. Yuan, H. Qi and C. Zhang, *Bioelectrochem.*, 81 (2011) 109.
20. T. Tsai, G. Heckert, L. F. Neves, Y. Tan, D. Kao, R.G. Harrison, D. E. Resasco, and D. W. Schmidtke, *Anal. Chem*, 81 (2009) 7917.
21. C. Deng, J. Chen and Z. Nie, S. Si, *Biosens. and Bioelectron.*, 26 (2010) 213.
22. M. A. Rahman, N. H. Kwon, M. S. Won, E. S. Choe and Y.B. Shim, *Anal. Chem*., 77 (2005) 4854.
23. H. Mugurauma, Y. Shibayama and Y. Matsui. *Biosens. Bioelectron*., 23 (2008) 827.
24. B. Lu and W. Chen, *J of Magn. and Magn. Materials*, 304 (2006) 400.
25. X. Jiang, Y. Wu, X. Mao, X. Cui and L. Zhu, *Sen and Actuat B*, 153 (2011) 158.
26. D. Wen, X. Zou, Y. Liu, L. Shang and S. Dong, *Talanta*, 79 (2009) 1233.
27. M. Ferreira, P. A. Fiorito, O. N. Oliveira, Jr and S. I. C. De Torresi, *Biosen. And Bioelectron*, 19 (2004) 1611.
28. A. Merkoci, M. Pumera, X. Llopis, B. Perez, M. del Valle and S. Alegret, *Trends in AnallChem*, 24 (2005) 826.

29. B. Y. Wu, S. H. Hou, F. Yin, J. Li, Z. X. Zhao, J. D. Huang and Q. Chen, *Biosen and Bioelectron*, 22 (2007) 838.
30. M. Tsai and Y. Tsai, *Sens. and Act. B*, 141 (2009) 592.
31. J. Lu, I. Do, L. T. Drzal, R. M. Worden and I. Lee, *ACS Nano*, 2 (2008) 1825.
32. V. L. Nguyen, M. Ohtaki, V. N. Ngo, M. T. Cao and M. Nogami, *Nanosci. Nanotechnol*, 3 (2012) 1
33. Y. Lin, C. Jiang, J. Xu, Z. Lin and V. V. Tsukruk. *Soft Matter*, 3 (2007) 432.
34. B. Chung, K. Kwon, S. Lee, J. Jin, C. H. Lee, C. E. Lee and Y. Park, *Adv. Mater*. 10 (1998) 1112.
35. F. N. Crespilho, F. Huguenin, V. Zucolotto**,** P. Olivi, F. C. Nart and O. N. Oliveira Jr, *ElectrochemCommun.*, 8 (2006) 348.
36. M. Handke and A. Kowalewska, *Spectrochimica. Acta*, 79 (2011) 749.
37. A. Kowalewska, W. Fortuniak and B. Handke, *J. Organomet. Chem.*, 694 (2009) 1345.
38. W. C. Liu, C. C. Yang, W. C. Chen, B. T. Dai and M. S. Tsai, *J. Non-Cryst.Solids*, 311 (2002) 233.
39. F. Huguenin, V. Zucolotto, A. J. F. Carvalho, E. R. Gonzalez, and O. N. Oliveira, Jr., *Chem. Mater*.,17 (2005) 6739.
40. R. M. Silverstein and F. X. Webster, *Spectrometric Identification of Organic Compounds*, Wiley-Interscience, New York, (1997).
41. C. Eiras, I. N. G. Passos, A. C. F. Brito, J. R. Santos,V. Zucolotto, O. N. Oliveira Jr, I. L. Kitagawa, C. J. L. Constantino and H. N. Cunha, *Quim Nova*. 30 (2007) 1158.
42. F. R. Dollish, W. G. Fateley and F. F. Bentley. *Characteristic Raman frequencies of organic compounds*, Wiley-Interscience, New York, (1974).
43. R. S. Freire, R. Peregrini, L. T. Kubota, N. Durán and P P. Zamora, *Quim. Nova*, 23 (2000) 504.
44. D. Sredni-Kenigsbuch, T. Kambayashi and G. Strassmann, *Immunol. Lett*., 71 (2000) 97.
45. L. Guo and D. H. Kim, *Chem. Commun.*, 47 (2011) 7125.
46. S. Prakash, T. Chakrabarty, A. K. Singh and V. K. Shahi, *Biosens. Bioelectron*, 41(2013) 43.
47. E. A. Ticianelli and E. R. Gonzalez. *"Eletroquímica – Princípios e Aplicações"*. 2ª. ed., Editora da Universidade de São Paulo – EDUSP, São Paulo, (2005) 220.
48. L. T. Kubota, J. C. Duarte, R. C. L. Silva, F. S. Damos and A. B. Oliveira, *J. Solid State Electrochem.*, 11 (2007) 631.
49. R. S. Nicholson and I. Shain, *Anal. Chem.*, 36 (1964) 06.
50. Q. Liu, X. B. Lu, J. Li, X. Yao and J. H. Li, *Biosens. Bioelectron*, 22 (2007) 3203.
51. Y. X. Huang, W. J. Zhang, H. Xiao and G. X. Li, *Biosens. Bioelectron*, 21 (2005) 817.
52. K. S Galhardo, R. M. Torresi and S. I. C. Torresi, *Electrochim. Acta*, 73 (2012) 123.
53. B. Li, D. T. Haynie, N. Palath and D. Janisch, *J of Nanosci and Nanotech*, 5 (2005) 1.
54. T. W. Tsai, G. Heckert, L. F. Neves, Y. Tan, D. Y. Kao, R. G. Harrison, D. E. Resasco and D. W. Schmidtke, *Anal. Chem.*, 81 (2009) 7917.
55. X. Ren, D. Chen, X. Meng, F. Tang, X. Hou, D. Han and L. Zhang, *J of Col. and Interf Sci*, 334 (2009) 183.
56. G. Reach and G. S, Wilson, *Anal. Chem*. 64, (1992) 381.
57. R.A. Kamin and G. S. Wilson, *Anal. Chem*, 52 (1980) 198.
58. A. Salimia and A. Noorbakhsh, *Electrochim. Acta*, 56 (2011) 6097.
59. I. L. De Mattos, L. V. Lukachova, L. Gorton, T. Laurell and A. A. Karyakin, *Talanta*, 54 (2001) 963.
60. H. Li, J. He, Y. Zhao, D. Wu, Y. Cai, Y.Q. Wei and M. Yang, *Electrochim. Acta*, 56 (2011) 2960.